

Article

## Part II: Oxidative Thermal Aging of Pd/Al<sub>2</sub>O<sub>3</sub> and Pd/Ce<sub>x</sub>O<sub>y</sub>-ZrO<sub>2</sub> in Automotive Three Way Catalysts: The Effects of Fuel Shutoff and Attempted Fuel Rich Regeneration

Qinghe Zheng <sup>1</sup>, Robert Farrauto <sup>1,\*</sup> and Michel Deeba <sup>2</sup>

<sup>1</sup> Earth and Environmental Engineering Department, Columbia University, 500 West 120th Street, New York, NY 10027, USA; E-Mail: qz2178@columbia.edu

<sup>2</sup> BASF Corporation, Research and Development Center, 25 Middlesex Essex Tpke, Iselin, NJ 08830-0770, USA; E-Mail: michel.deeba@basf.com

\* Author to whom correspondence should be addressed; E-Mail: rf2182@columbia.edu; Tel.: +1-212-854-6390; Fax: +1-212-854-7081.

Academic Editor: Jae-Soon Choi

Received: 30 August 2015 / Accepted: 8 October 2015 / Published: 23 October 2015

---

**Abstract:** The Pd component in the automotive three way catalyst (TWC) experiences deactivation during fuel shutoff, a process employed by automobile companies for enhancing fuel economy when the vehicle is coasting downhill. The process exposes the TWC to a severe oxidative aging environment with the flow of hot (800 °C–1050 °C) air. Simulated fuel shutoff aging at 1050 °C leads to Pd metal sintering, the main cause of irreversible deactivation of 3% Pd/Al<sub>2</sub>O<sub>3</sub> and 3% Pd/Ce<sub>x</sub>O<sub>y</sub>-ZrO<sub>2</sub> (CZO) as model catalysts. The effect on the Rh component was presented in our companion paper Part I. Moderate support sintering and Pd-Ce<sub>x</sub>O<sub>y</sub> interactions were also experienced upon aging, but had a minimal effect on the catalyst activity losses. Cooling in air, following aging, was not able to reverse the metallic Pd sintering by re-dispersing to PdO. Unlike the aged Rh-TWCs (Part I), reduction via *in situ* steam reforming (SR) of exhaust HCs was not effective in reversing the deactivation of aged Pd/Al<sub>2</sub>O<sub>3</sub>, but did show a slight recovery of the Pd activity when CZO was the carrier. The Pd<sup>+</sup>/Pd<sup>0</sup> and Ce<sup>3+</sup>/Ce<sup>4+</sup> couples in Pd/CZO are reported to promote the catalytic SR by improving the redox efficiency during the regeneration, while no such promoting effect was observed for Pd/Al<sub>2</sub>O<sub>3</sub>. A suggestion is made for improving the catalyst performance.

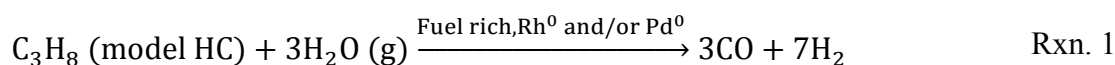
**Keywords:** automotive three way catalysts (TWC); Pd/Al<sub>2</sub>O<sub>3</sub>; Pd/Ce<sub>x</sub>O<sub>y</sub>-ZrO<sub>2</sub>; fuel shutoff aging; catalyst deactivation; fuel rich regeneration; metal sintering; metal-support interaction

---

## 1. Introduction

The modern three way catalyst (TWC) for automotive emission control is bimetallic Rh-Pd supported on stabilized  $\gamma$ -Al<sub>2</sub>O<sub>3</sub>. Under stoichiometric air-to-fuel ratio, the TWC allows simultaneous conversion of engine exhaust pollutants (NO<sub>x</sub>, CO, and HCs) into innocuous N<sub>2</sub>, CO<sub>2</sub>, and H<sub>2</sub>O, respectively. A companion article (Part 1) provides more details on the background of the TWC technology.

The catalyst experiences severe deactivation during the fuel shutoff process, an automotive strategy for enhancing fuel economy by discontinuing the fuel flow when the vehicle is coasting downhill. This process deactivates the TWC by exposure to a high-temperature (800 °C–1050 °C) oxidizing environment. A subsequent return of engine operation to slightly fuel rich conditions allows almost complete regeneration of Rh-TWC by reduction of the oxidized Rh species. H<sub>2</sub> generated through *in situ* steam reforming (SR) of exhaust HCs (*i.e.*, C<sub>3</sub>H<sub>8</sub>), is catalyzed by the Rh and Pd metal sites remaining active (Rxn. 1). The mode of operation has been practiced in the automotive industry for a number of years. Our research objective is to study the reaction mechanism and the catalyst surface physicochemistry during both the aging and the attempted regeneration processes for the Pd component in the TWC.



Our research report is divided into two parts, with focus on Rh- (Part I) and Pd- (Part II) TWCs both supported on  $\gamma$ -Al<sub>2</sub>O<sub>3</sub> or Ceria-Zirconia (denoted as CZO). The influence of simulated fuel shutoff aging and attempted catalyst regeneration on the catalyst performance and the catalyst surface physicochemistry were examined. Part I reveals that the Rh-support interactions were the major cause of catalyst deactivation and could be reversed by this reduction/regeneration procedure consistent with current vehicle operation.

The present Part II study reports the stability of Pd/Al<sub>2</sub>O<sub>3</sub> and Pd/Ce<sub>x</sub>O<sub>y</sub>-ZrO<sub>2</sub> as model catalysts for automotive TWC during simulated fuel shutoff aging and attempted fuel rich regeneration cycle tests. The study examines the effect of the fuel rich conditions on Pd-TWC, an effective approach for maintaining the catalytic performance of Rh-TWC. The catalytic activity tests were performed in combination with catalyst characterization measurements including XRD, BET surface area, TEM, and H<sub>2</sub>-TPR to correlate the catalyst performance to the catalyst property after aging/attempted regeneration.

## 2. Results and Discussion

### 2.1. Aging-Induced Pd Sintering: The Primary Catalyst Deactivation Mode

Figure 1 compares the activity of the fresh and aged Pd catalysts as measured by steam reforming H<sub>2</sub> production (mol % in the product) at simulated fuel rich condition. Generally, catalyst deactivation was modest at the lower aging temperature (800 °C), but was accelerated with increasing aging temperature up to 1050 °C. The extent of deactivation varied with the support material. The reforming activity for

Pd/Al<sub>2</sub>O<sub>3</sub> showed little change after 800 °C aging. In contrast, Pd/CZO continuously deactivated as the aging temperature increased. The SR conversion losses at 350 °C for Pd/Al<sub>2</sub>O<sub>3</sub> and Pd/CZO were respectively 59.67% and 72.29% after aging at 1050 °C.

The catalyst activity after attempted regeneration (reduction by SR at simulated fuel rich condition) is compared in Figure 2. Attempted regeneration was not very effective in restoring the activity of Pd catalysts, with no gain in activity for 3% Pd/Al<sub>2</sub>O<sub>3</sub> and a modest conversion increase for 3%/CZO shown. Table 1 summarizes the  $T_{50s}$  (temperature at which 50% maximum equilibrium H<sub>2</sub> production is reached during activity tests) of the Pd catalysts before and after aging/attempted regeneration, in comparison with the Rh catalysts. It is clear that the deactivated Rh catalysts were essentially fully regenerated while Pd catalysts were not. Clearly supported Rh and Pd have different deactivation modes.

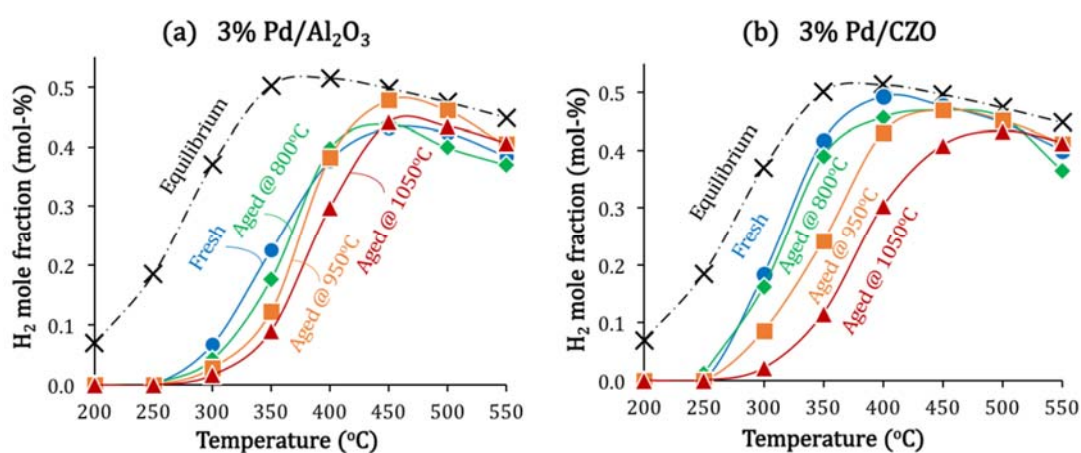


**Figure 1.** Activity of fresh and aged (a) 3% Pd/Al<sub>2</sub>O<sub>3</sub> and (b) 3% Pd/CZO in converting simulated engine exhaust gas at fuel rich condition. Catalyst activity is plotted in terms of H<sub>2</sub> product mole fraction as a function of reaction temperature (200 °C to 550 °C). Aged catalysts were obtained by treating fresh ones in air at 800 °C, 950 °C, or 1050 °C for 5 min, followed by cooling to room temperature in air.

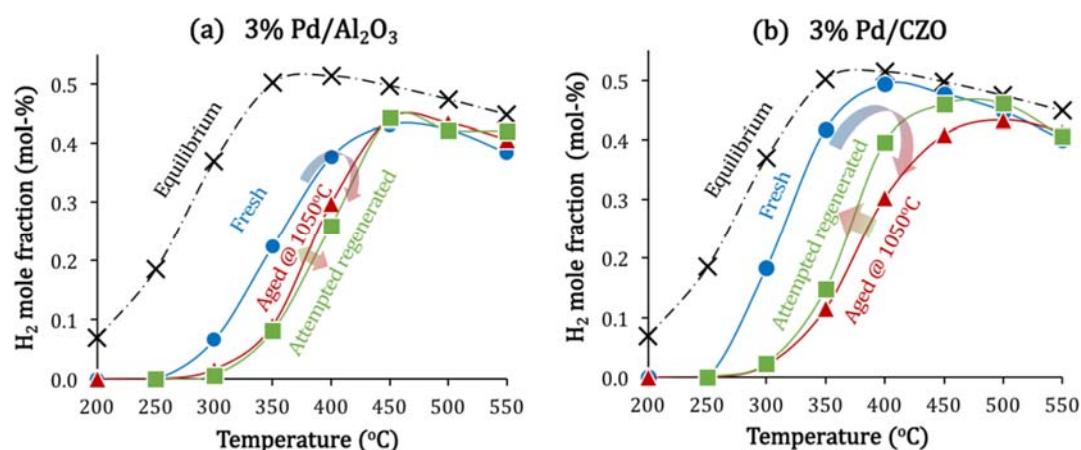


**Figure 2.** Activity of fresh, aged, and attempted regenerated (a) 3% Pd/Al<sub>2</sub>O<sub>3</sub> and (b) 3% Pd/CZO in converting simulated engine exhaust gas at fuel rich condition. Aged catalysts were obtained by treating fresh ones in air at 1050 °C for 5 min, followed by cooling to room temperature in air. Attempted catalyst regenerations were performed by SR at rich condition at 550 °C for 1 h.

**Table 1.**  $T_{50s}$  (°C) of fresh, aged, and attempted regenerated 3% Pd/Al<sub>2</sub>O<sub>3</sub> and 3% Pd/CZO, in comparison with 0.5% Rh/Al<sub>2</sub>O<sub>3</sub> and 0.5% Rh/CZO as reported in Part I.

Catalyst	Fresh	After Aging in Air for 5 min at Different T			After Attempted Regeneration *
		800 °C	950 °C	1050 °C	
0.5% Rh/Al <sub>2</sub> O <sub>3</sub>	375	415	460	470	375
0.5% Rh/CZO	334	365	431	435	330
3% Pd/Al <sub>2</sub> O <sub>3</sub>	360	367	375	390	390
3% Pd/CZO	315	320	355	387	370

Annotation: \* Attempted catalyst regenerations were performed at 550 °C in propane-containing feed gas.

The aging study was extended to multiple cycles consistent with the vehicle operations. The activity of both catalysts after every five cycles of aging-attempted regeneration are plotted in Figure 3. Continuous losses in the catalyst ability to be regenerated were observed with increasing number of cycles. The regenerability of Pd/CZO was always slightly greater than Pd/Al<sub>2</sub>O<sub>3</sub> in each cycle, based on the lower temperature for H<sub>2</sub> conversion and its larger slope. However, continuous catalyst deactivation was experienced by Pd/CZO even up to 20 cycles of aging. In comparison, Pd/Al<sub>2</sub>O<sub>3</sub> seemed to stabilize at five cycles and beyond.

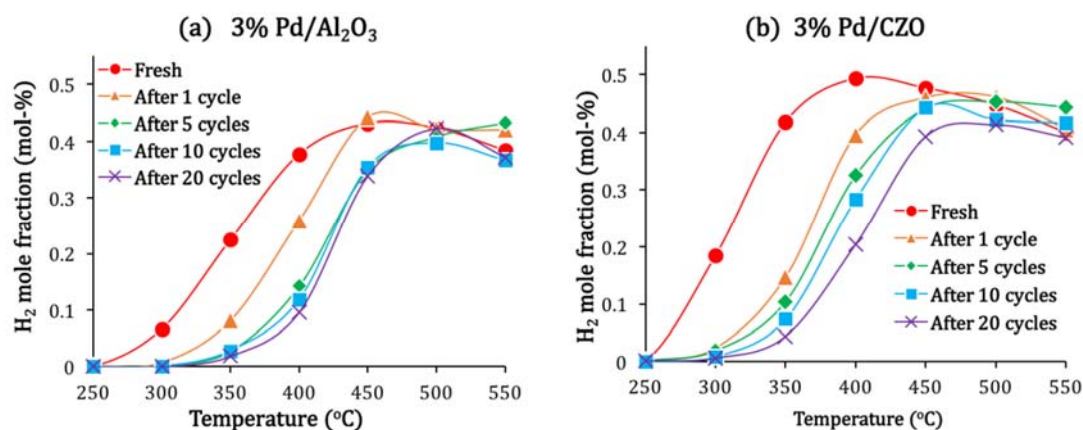


**Figure 3.** Activity of attempted regenerated (a) 3% Pd/Al<sub>2</sub>O<sub>3</sub> and (b) 3% Pd/CZO catalysts after 1, 5, 10, and 20 cycles in the aging-regeneration cycle tests. After every five cycles of aging/regeneration. The catalyst activity is plotted in terms of H<sub>2</sub> product mole fraction as a function of SR temperature from 250 °C to 550 °C.

Figure 4 shows the H<sub>2</sub> production vs. time on stream (TOS) during the attempted regeneration in the first five cycles for both Pd catalysts. For 3% Pd/Al<sub>2</sub>O<sub>3</sub>, no enhancement in SR performance was observed for each attempted regeneration cycle, confirming that the Pd/Al<sub>2</sub>O<sub>3</sub> is non-regenerable by this treatment. For 3% Pd/CZO, the SR performance was observed to slowly increase indicating a slight recovery of catalyst activity.

These results indicate similar deactivation mechanisms for the two catalysts but a small regenerating effect for Pd/CZO was observed. TEM studies will confirm that Pd sintering is a major cause of deactivation.

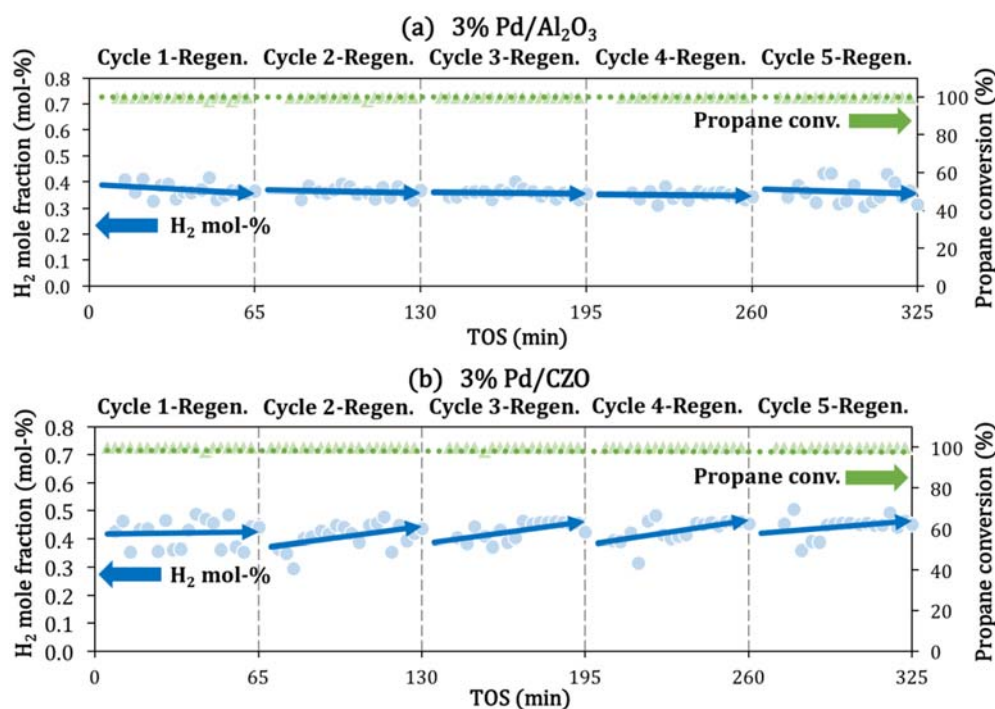


**Figure 4.** H<sub>2</sub> productions as a function of time on stream (TOS) during attempted regeneration processes in simulated fuel shutoff aging-attempted fuel rich regeneration cycle tests (First 5 cycles out of total 25 cycles) with (a) 3% Pd/Al<sub>2</sub>O<sub>3</sub> and (b) 3% Pd/CZO. In each cycle, the catalyst sample was first aged in air at 1050 °C for 5 min, followed by attempted *in situ* regeneration at fuel rich condition at 550 °C for 1 h.

Previous studies reported that Pd metal sintering was prominent at high temperature ( $\geq 800$  °C), and was a major contributor to Pd catalyst deactivation [1–4]. Upon aging at 1050 °C, metal sintering occurred for both of our Pd catalysts. Metal sintering in Pd/Al<sub>2</sub>O<sub>3</sub> was more or less complete after multiple aging-regeneration cycles ( $>10$  Cycles), leading to relatively stable catalyst performance. In contrast, metal sintering also occurred in Pd/CZO, but continued with each cycle resulting in a continuous decrease in catalyst activity. Metal sintering in aged Pd/CZO is more difficult to be stabilized than for Pd/Al<sub>2</sub>O<sub>3</sub>.

It is useful to mention that even though CZO has some steam reforming activity especially at high reaction temperature, Pd is always the active sites in the *in situ* catalyst regeneration. In another measurement (Figure 5), it is shown that the catalytic steam reforming activity increased dramatically with Pd loaded, compared to that of the CZO support-only.

Significant Pd metal sintering, after aging, was observed by TEM measurements, with representative images presented in Figure 6, and TEM-derived metal particle size distributions of 3% Pd/Al<sub>2</sub>O<sub>3</sub> and 3% Pd/CZO catalysts before and after aging and attempted regeneration are shown in Figure 7. The Pd and support (Al<sub>2</sub>O<sub>3</sub> or CZO) crystals are differentiated by their distinct shapes, crystallite size, and electron transmission ability. Pd/support (Al<sub>2</sub>O<sub>3</sub> or CZO support) crystallographic structure was previously identified by the dark particles distributed on light background in their TEM images [5–8]. The electron scattering intensity from thin specimens follows the  $Z^2$  dependence of Rutherford's law, where  $Z$  is the atomic number. For example, one Pt atom scatters as strongly as about 100 oxygen atoms or 32 silicon atoms. The technique is highly successful in detecting clusters of catalytic active metals such

as Pt, Pd, or Rh, on light supports such as zeolites, or mesoporous silica and alumina [9]. It should be admitted that the metal-support contrast can also be affected by the exposed crystallite plane orientation. The crystallite shapes and sizes are therefore used to facilitate differentiation of the Pd metal from the support. In our TEM result, fresh Pd/Al<sub>2</sub>O<sub>3</sub> (Figure 6a) is characterized by well-dispersed dark spherical spots (Pd metal) with a narrow range of small diameters (with mean Feret diameter of 4.08 nm) supported on needle-like Al<sub>2</sub>O<sub>3</sub> crystal. Fresh Pd/CZO (Figure 6d) is characterized by visible faceted spherical spots (Pd metal) with a mean Feret diameter of 5.73 nm, supported on cubic shaped Ce<sub>x</sub>O<sub>y</sub> crystallite structure with ZrO<sub>2</sub> incorporated.

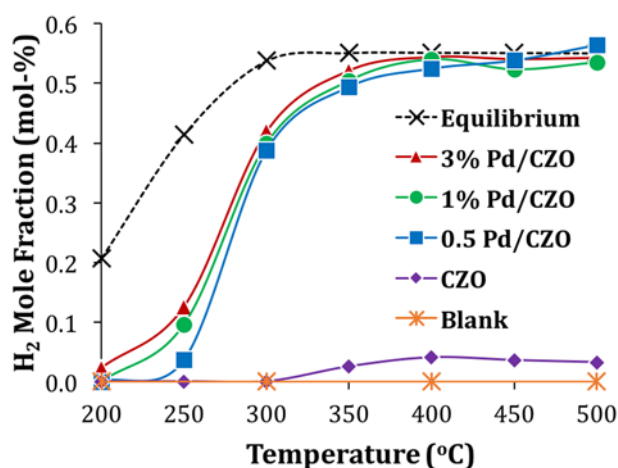


**Figure 5.** Activity of fresh Pd/CZO catalysts with different metal loadings (0%, 0.5%, 1%, and 3%) in converting simulated engine exhaust gas at fuel rich condition. Catalyst activity is plotted in terms of H<sub>2</sub> product mole fraction as a function of reaction temperature (200 °C to 550 °C). Reaction feed: 500 ppm propane, 10% H<sub>2</sub>O, and N<sub>2</sub> balance, with total GHSV of 30,000 h<sup>-1</sup>.

After 1050 °C aging, significant Pd sintering was observed in the TEM images showing increased crystallite sizes. The metal size distributions of Pd/Al<sub>2</sub>O<sub>3</sub> (Figure 6b) and Pd/CZO (Figure 6e) shifted to higher values, with predominant particle sizes of 10–12 nm and maxim particle diameter up to 20 nm. Ostwald Ripening has been reported to be the dominant process causing the growth of Pd nanoparticles leading to losses of metal surface area and catalyst activity [10]. After attempted regeneration (Figure 6c,f), little change in the crystallite size distributions were found, proving that the regeneration method was neither effective in reversing metal sintering, or causing any further catalyst deactivation.

Consistent with a recent study by Chen *et al.* [11], Pd metal sintering was the principle mode of catalyst deactivation when Al<sub>2</sub>O<sub>3</sub> was the support upon thermal oxidation. Compared to metal sintering, the authors claim support phase change and Pd-Al<sub>2</sub>O<sub>3</sub> interactions were less significant and less responsible for catalyst deactivation.

Farrauto, *et al.* [12], found in 1992, that well dispersed PdO on Al<sub>2</sub>O<sub>3</sub> decomposes to Pd at 800 °C in air in two distinct steps. The first step occurs between 750 °C and 800 °C, and a second decomposition happens between 800 °C and 850 °C, causing a greater extent of Pd sintering and agglomeration. Subsequent cooling in air below 650 °C causes some re-dispersion with the formation of a surface rich in PdO<sub>x</sub> (PdO<sub>x</sub>-Pd/Al<sub>2</sub>O<sub>3</sub>). The re-dispersion model was confirmed by Datye, *et al.* [13], who further

demonstrated that PdO decomposition at higher temperatures ( $>800$  °C) leads to re-dispersion being more difficult. The hysteresis (temperature difference) for decomposition and reformation is also strongly dependent on the nature of the support material [14,15], in the following decreasing order:  $ZrO_2 > Al_2O_3 > Ta_2O_5 > TiO_2 > CeO_2$ . Compared to PdO/ $Al_2O_3$ , there exists a large region of temperature stability of the PdO when dispersed on  $CeO_2$ . However, the aging temperature (1050 °C) in our study was much higher than previously reported. Therefore, attempted re-dispersion upon air-cooling was not effective in reversing the severe Pd sintering. Clearly if PdO could be stabilized against decomposition to Pd above 800 °C, extensive sintering would not likely occur. Some advances in this concept have been reported in a US patent in which PdO forms a binary oxide with praseodymium [16]. These materials are stable above 1000 °C however do sacrifice some activity relative to PdO only. A stable PdO suggests that decreases in the amount of Rh in the TWC might be possible since Pd has good  $NO_x$  activity. Its high  $NO_x$  activity was exploited in the mid-1990s when all Pd catalysts (Rh free) were commercialized in TWC when regulations were not as demanding as they are today [17].

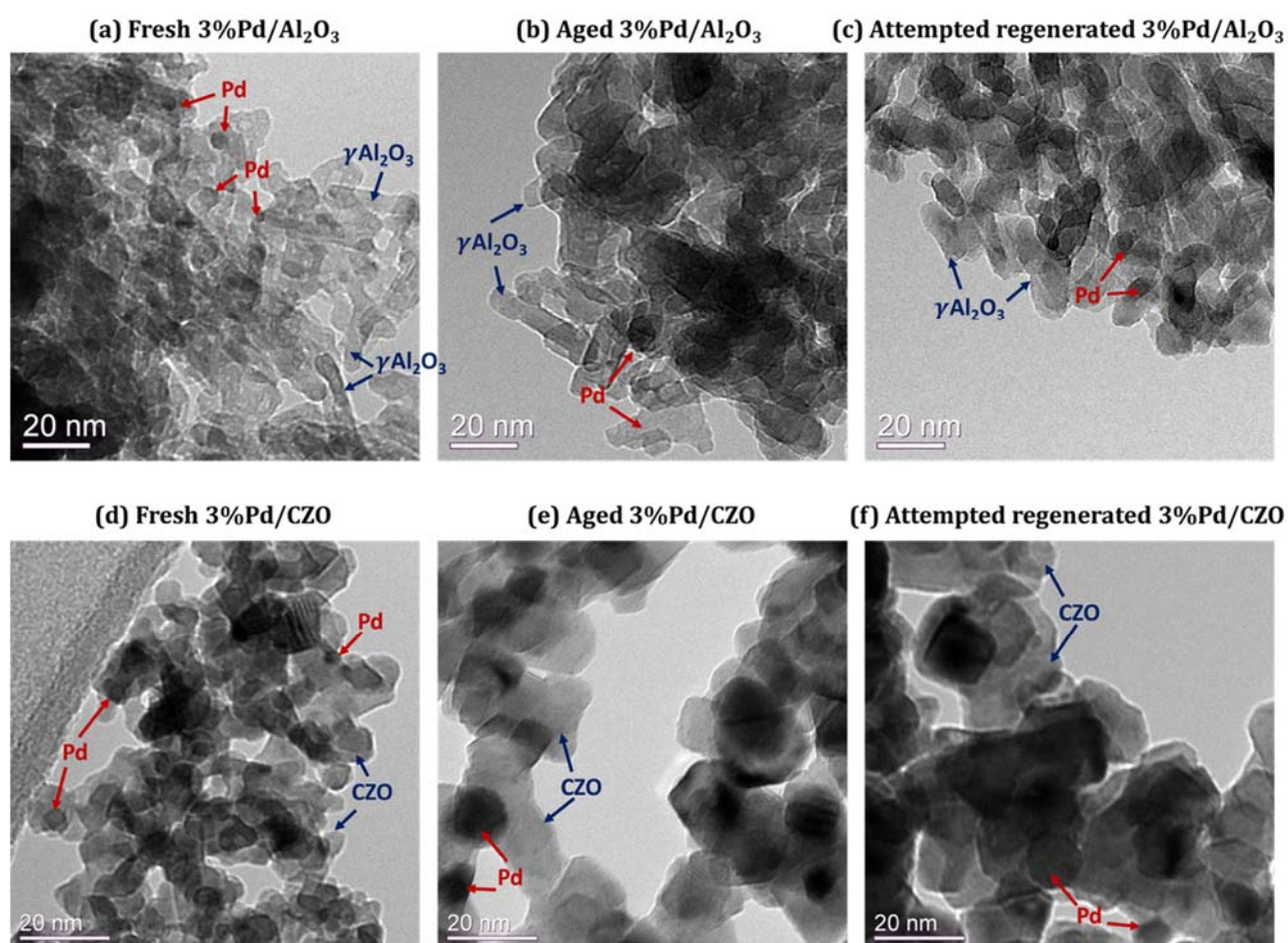


**Figure 6.** Representative TEM images of fresh, aged, and attempted regenerated 3% Pd/ $Al_2O_3$  (a–c) and 3% Pd/CZO (d–f). Aged samples were achieved by aging the fresh catalyst in air or  $N_2$  at 1050 °C for 5 min. Attempted catalyst regenerations were performed by at rich condition at 550 °C for 1 h.

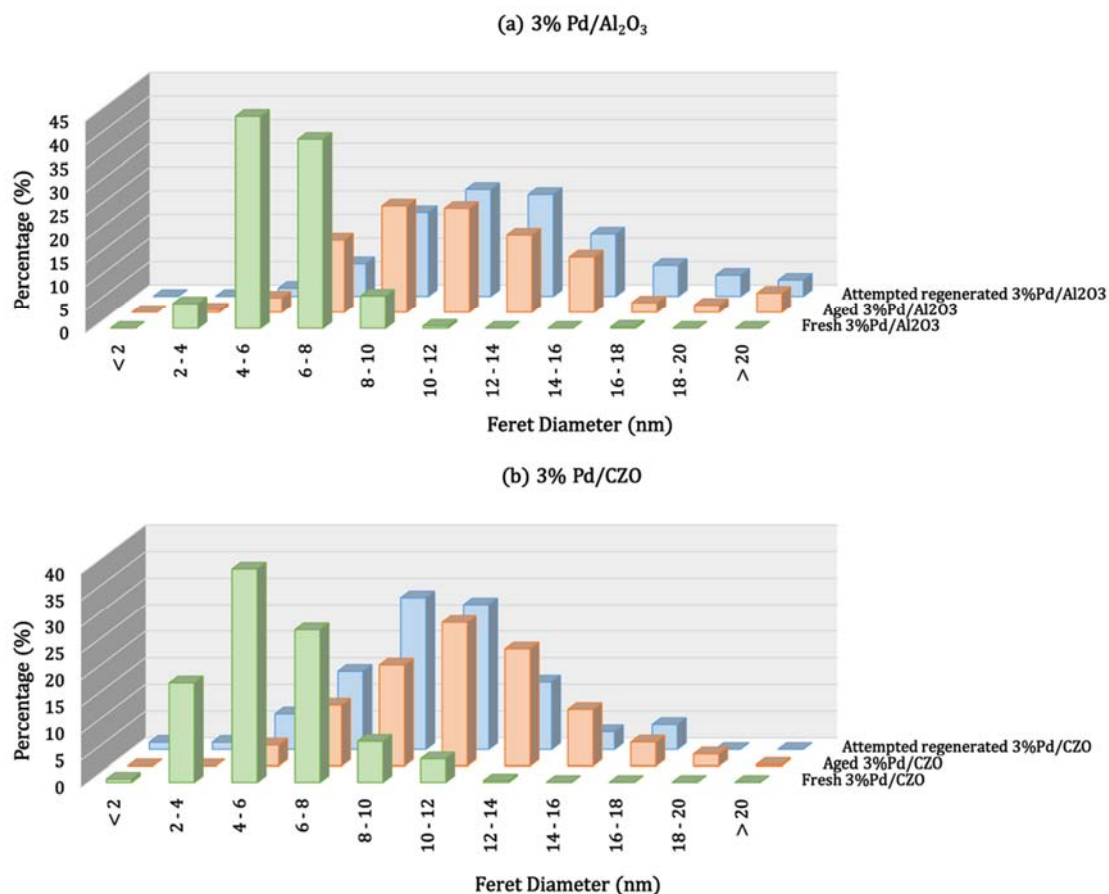


**Figure 7.** TEM-derived Pd metal particle size distributions of fresh, aged, and attempted regenerated (a) 3% Pd/Al<sub>2</sub>O<sub>3</sub> and (b) 3% Pd/CZO. Aging and attempted regeneration conditions were as described in Figure 6.

Metal sintering and metal-support interactions (Pd–O–Ce) are suggested as the two causes of catalyst deactivation for Pd/CZO. Only the metal-support interactions (Pd–O–Ce) could be slightly reversed by regeneration. The slightly enhanced activity of Pd/CZO after attempted regeneration, was likely attributed to the enhanced redox between Pd<sup>+</sup>/Pd<sup>0</sup> and Ce<sup>4+</sup>/Ce<sup>3+</sup> couples. Similar to Rh, Pd was reported to promote the transformation of Ce<sup>4+</sup> to Ce<sup>3+</sup> when deposited on CZO [18]. Due to the higher energy potential of the Ce<sup>4+</sup>/Ce<sup>3+</sup> redox couple (1.61 eV) than that of the Pd<sup>2+</sup>/Pd<sup>0</sup> (0.915 eV), oxygen vacancies form easily and act as the enhancement of oxygen spillover and back-spillover processes at the Pd/CZ interfaces [19]. The formation of Pd<sup>+</sup>/Pd<sup>0</sup>-Ce<sup>4+</sup>/Ce<sup>3+</sup> redox couples therefore benefits the oxygen-buffering effect, and facilitates molecular bond dissociation during catalytic reactions [20–24].

## 2.2. Support Sintering and Pd-Support Interaction: Other Catalyst Deactivation Modes

Support sintering occurred for both Al<sub>2</sub>O<sub>3</sub> and CZO and was accelerated with increasing aging temperature, as indicated by the sharp decreases in BET surface area (Figure 8). Most significant losses in surface areas occurred above 950 °C (IV in Figure 8). Aging at >950 °C for a 5 min period introduced measurable sintering of Al<sub>2</sub>O<sub>3</sub>, but was insufficient for the phase transformation of  $\gamma$ -Al<sub>2</sub>O<sub>3</sub> to  $\theta$ -Al<sub>2</sub>O<sub>3</sub> [25,26]. CZO sintering was previously reported accelerated in the presence of supported Pd [27]. Even though the extent of support sintering after high temperature (1050 °C) aging was

significant metal encapsulation was negligible as confirmed by TEM (Figure 6). The observed crystallite sizes of the sintered Pd metal and Al<sub>2</sub>O<sub>3</sub> or CZO support were comparable in aged samples. After 1050 °C aging, metal sintering was sufficient and the enlarged Pd particles were not able to be encapsulated by support crystals with similar sizes.

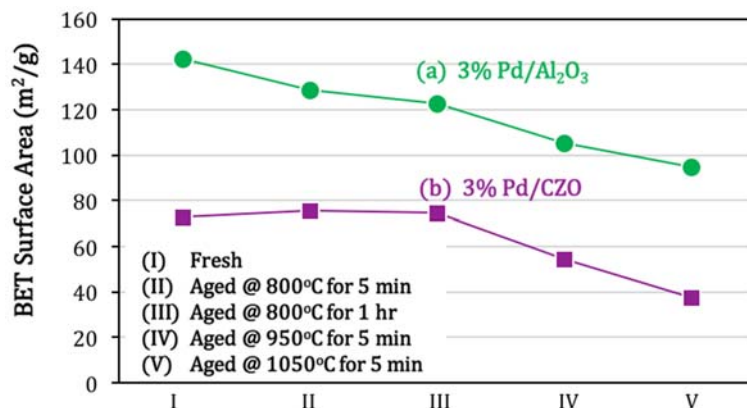


**Figure 8.** BET surface areas of fresh and aged (a) 3% Pd/Al<sub>2</sub>O<sub>3</sub> and (b) 3% Pd/CZO, as a function of aging conditions. Aged samples were obtained by aging the (I) fresh catalysts in air at the following conditions: (II) 800 °C for 5 min, (III) 800 °C for 1 h, (IV) 950 °C for 5 min, or (V) 1050 °C for 5 min. The aging processes were followed by cooling in air to room temperature. As a reference, BET surface areas of support materials were measured 142.9 m<sup>2</sup>/g and 60.3 m<sup>2</sup>/g respectively for fresh Al<sub>2</sub>O<sub>3</sub> and CZO.

Powder X-ray diffraction (XRD) was used to investigate the phase structures of the fresh and aged 3% Pd/Al<sub>2</sub>O<sub>3</sub> and 3% Pd/CZO catalysts. The XRD patterns of the 3% Pd/Al<sub>2</sub>O<sub>3</sub> samples are shown in Figure 9a,b, with XRD peaks indexed to three phases, *i.e.*,  $\gamma$ -Al<sub>2</sub>O<sub>3</sub>, Pd, and PdO. Well-structured tetragonal  $\gamma$ -Al<sub>2</sub>O<sub>3</sub> are characterized by exclusive (220), (311), (400), and (440) reflections and invariable (111), (222), (511), (444) planes. In agreement with the BET result, sintering of the Al<sub>2</sub>O<sub>3</sub> support is confirmed by increased crystallite size as confirmed by the Scherrer Equation. The visibility of metal/metal oxide XRD patterns is improved by aging, due to extensive metal sintering experienced by Palladium. The XRD patterns of the tetragonal PdO and cubic Pd crystallite structures in aged samples are visible but are of relative low intensity due to the low metal loading (3%) and small crystallite size. Consistent with literature [12], PdO is formed during the air cooling. The most significant reflections of aged PdO are (110), (112), and (211). The Pd peaks including (111) and (200) partially overlap with the Al<sub>2</sub>O<sub>3</sub> patterns, and are only identifiable in aged samples.

The XRD patterns of the fresh and aged 3% Pd/CZO are shown in Figure 9c,d, with zoomed view of the aged Pd/PdO-related patterns shown at the bottom of Figure 1. Based on our observation and a previous report [28], it can be concluded that most of the Zr incorporated into the CeO<sub>2</sub> phase forms a Zr<sub>x</sub>Ce<sub>1-x</sub>O<sub>2</sub> solid solution of cubic symmetry, where *x* is equal to the actual Zr loading (~67%). Similar to Pd/Al<sub>2</sub>O<sub>3</sub> samples, significant sintering of both the metal and the support are suggested by Scherrer equation after aging.

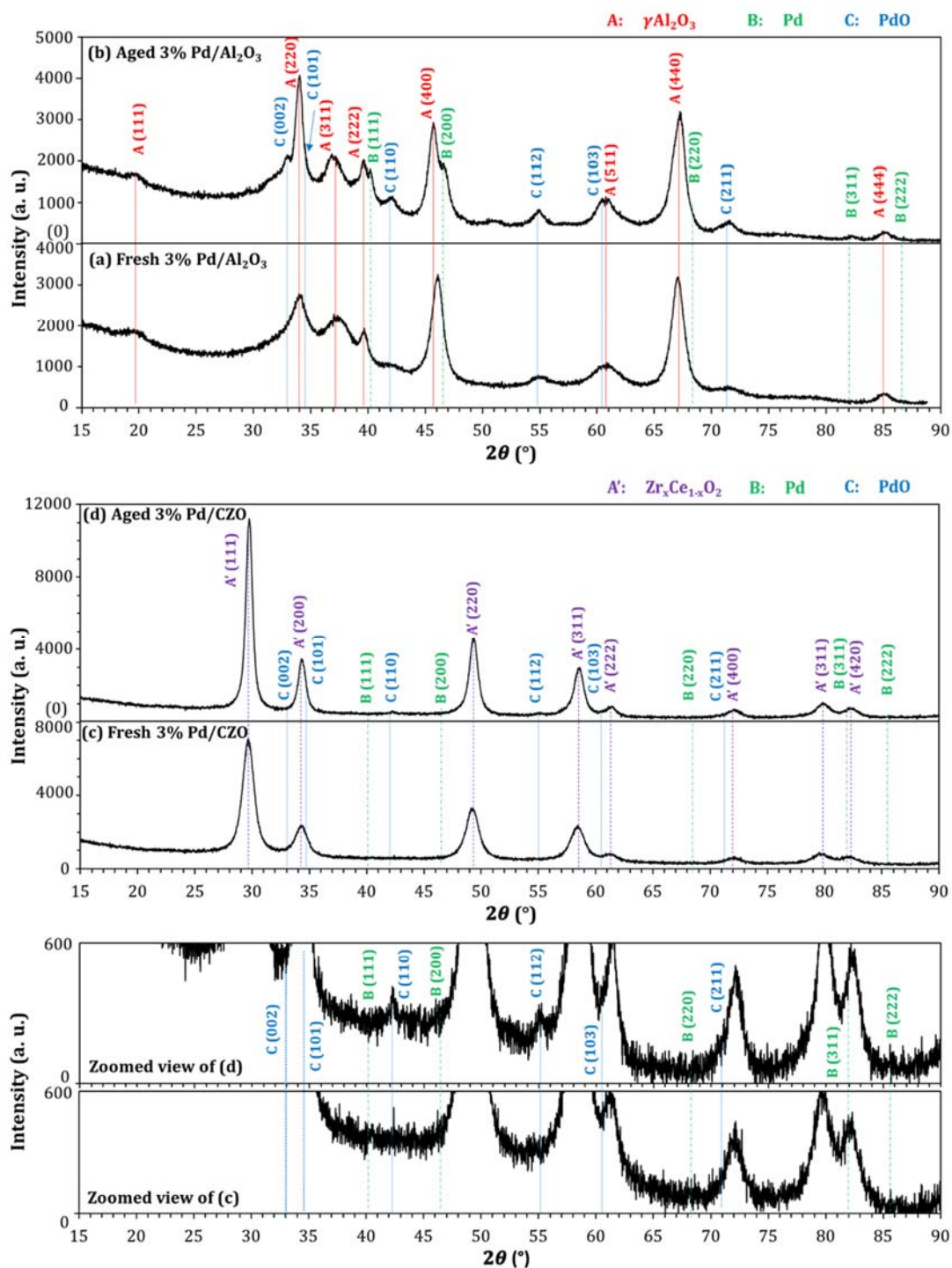


**Figure 9.** X-ray diffraction (XRD) patterns for (a) Fresh 3% Pd/Al<sub>2</sub>O<sub>3</sub>; (b) Aged 3% Pd/Al<sub>2</sub>O<sub>3</sub>, (c) Fresh 3% Pd/CZO; (d) Aged 3% Pd/CZO; and the zoomed views of (c,d). Aging condition: 1050 °C in air for 5 min. XRD patterns were obtained by using Cu-K $\alpha$ 1 radiation ( $\lambda = 1.5406 \text{ \AA}$ ).

The mean metal and support crystallite size analyses by XRD and TEM are compared in Table 2. The full-width at half maxima of the (400) and (111) peaks of respectively the  $\gamma$ -Al<sub>2</sub>O<sub>3</sub> and CZO phases are used for the support crystallite size calculations. PdO (110) peak is used for the metal crystallite size calculations for the aged samples for both Al<sub>2</sub>O<sub>3</sub> and CZO supports. The fresh metal crystallite sizes

cannot be detected. The crystallite size results are consistent for both the XRD and TEM. Compared to CZO support, Al<sub>2</sub>O<sub>3</sub> presents more refractory nature towards thermal oxidative aging, which is in agreement with the BET result.

**Table 2.** Support mean crystallite sizes of the fresh and aged (1050 °C in air for 5 min) 3% Pd/Al<sub>2</sub>O<sub>3</sub> and 3% Pd/CZO measured by TEM and XRD.

Catalyst		Metal Crystallite Size (nm)		Support Crystallite Size (nm)	
		XRD	TEM	XRD	TEM
Fresh 3% Pd/Al <sub>2</sub> O <sub>3</sub>	Fresh	--	4.1	7.2	7.0
	Aged	10.3	11.3	7.7	7.4
Fresh 3% Pd/CZO	Fresh	--	5.7	7.3	6.5
	Aged	12.9	11.2	12.6	12.0

The H<sub>2</sub>-TPR profiles of Pd catalysts are profiled with normalized H<sub>2</sub> consumption as a function of programmed temperature in Figure 10. A negative H<sub>2</sub> consumption peak (release of H<sub>2</sub>) around 71 °C were ascribed to the release of hydrogen from palladium hydride β-PdH<sub>x</sub> [29–31]. β-PdH<sub>x</sub> was formed during H<sub>2</sub> purge prior to TPR analysis (to achieve TPR baseline), when H<sub>2</sub> was absorbed by metastable Pd crystallite particles at ambient temperature. The peak correlated well with the average PdO crystallite size, since the hydride formation is a bulk phenomenon [32]. The larger amount of H<sub>2</sub> released with increasing aging temperature indicates the existence of larger size Pd crystallites with a greater capacity for adsorbing H<sub>2</sub> via hydride formation. This further supports the Pd metal sintering observation.

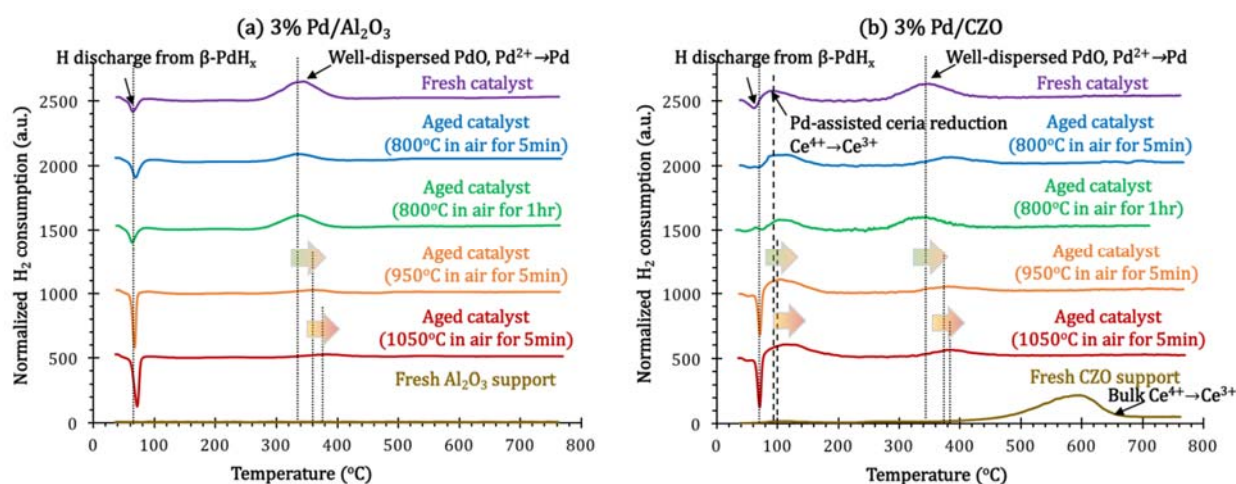


**Figure 10.** Normalized H<sub>2</sub> consumption in H<sub>2</sub>-Temperature Programmed Reduction (H<sub>2</sub>-TPR) measurements of fresh and aged (a) 3% Pd/Al<sub>2</sub>O<sub>3</sub> and (b) 3% Pd/CZO, as a function of reducing temperature. Aged samples for measurements were respectively achieved by aging the fresh ones in air at the following conditions: 800 °C for 5 min, 800 °C for 1 h, 950 °C for 5 min, or 1050 °C for 5 min.

Pd reduction peaks at higher temperatures (~300 °C) were observed for both catalysts, and were either assigned to the hydrogen consumption by a spillover from Pd to the support material [33,34], or to the reduction of stable PdO<sub>x</sub> species in intimate contact with the support [35]. In either case, high temperature-H<sub>2</sub> consumption is attributed to the interactions between the well dispersed PdO<sub>x</sub> species

and the ceria support. The existence of Pd–O–Ce interaction is evident by both the TPR and the activity results. Note that during attempted regeneration, Pd–O–Ce interaction could be partially reversed assisted by the  $\text{Pd}^{x+}/\text{Pd}^0$  and  $\text{Ce}^{4+}/\text{Ce}^{3+}$  redox couples, while Pd/ $\text{Al}_2\text{O}_3$  showed no detectable regeneration. Compared to the low temperature reducible PdO crystallites as mentioned before, the  $\text{PdO}_x$  particles in close contact with the support have smaller crystallite size. The number of the interactive  $\text{PdO}_x$  particles decreased by being “agglomerated” into the larger PdO, creating a more sintered particle with a decrease in the high temperature  $\text{H}_2$  consumption. However, the intensity of the metal-support interaction became stronger, as indicated by the shift of the reduction temperature to even higher temperature.

The interaction of Pd with  $\text{CeO}_2$  in intimate contact enhances the reducibility of the support [36], and positively influences the redox state of the active metal [37–40]. For fresh and aged Pd/CZO, the TPR peaks observed between 100 °C and 120 °C are attributed to the reduction of  $\text{Ce}^{4+}$  to  $\text{Ce}^{3+}$  assisted by Pd. In comparison, the reduction of ceria for CZO support (no Pd present) occurs at much higher temperature (~600 °C). With increasing aging temperature, the Pd-assisted reduction of ceria becomes more difficult as evident by the increased reducing temperature due to the loss of well dispersed Pd particles (in intimate contacts with  $\text{CeO}_2$ ) consumed by the sintering process.

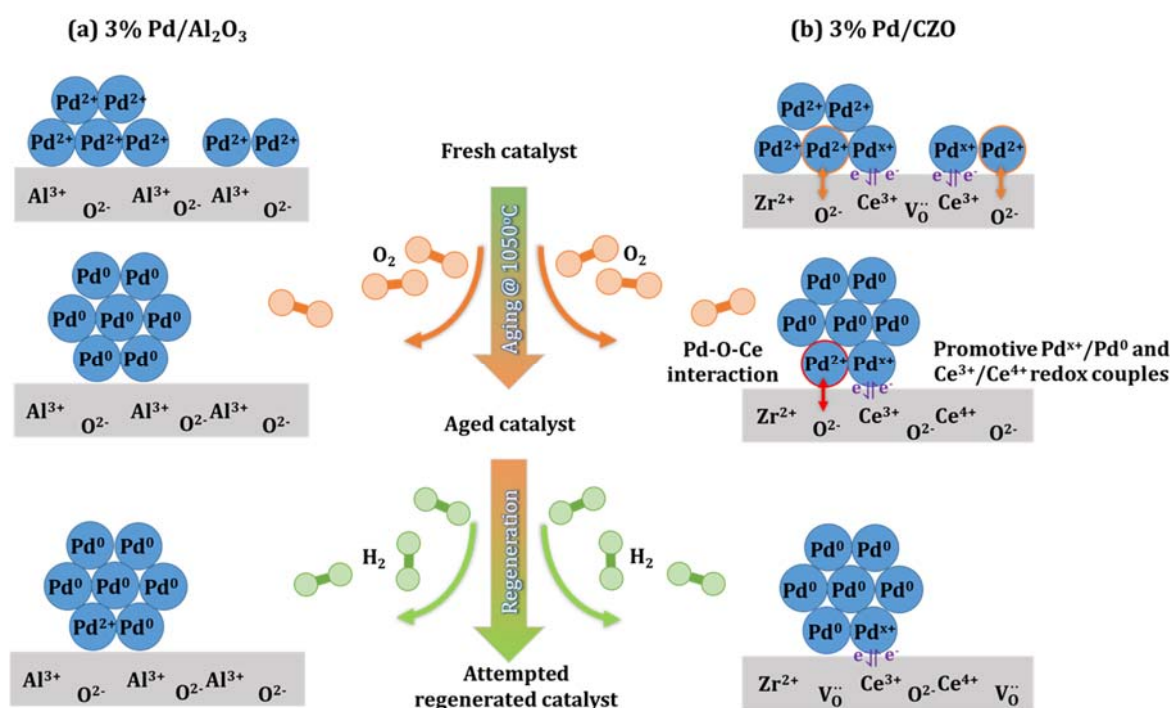


**Figure 11.** Schematic of proposed model for deactivation and regeneration of 3% Pd/ $\text{Al}_2\text{O}_3$  and 3% Pd/CZO during simulated fuel shutoff aging (1050 °C) and fuel rich regeneration (550 °C).

The proposed deactivation and attempted regeneration mechanisms for 3% Pd/ $\text{Al}_2\text{O}_3$  and 3% Pd/CZO after aging at 1050 °C and the fuel rich  $\text{H}_2$  treatment (550 °C) is sketched in Figure 11. For Pd on both supports, metal sintering was the main cause of catalyst deactivation. The aging temperature was sufficiently high for PdO decomposition to Pd, leading to significant metal sintering. Subsequent cooling was unable to reverse sintering via PdO reformation or re-dispersion. Aging also led to modest

Pd–O–Ce interactions, which occurred mostly at the Pd/Ce<sub>x</sub>O<sub>y</sub> interfaces. The Pd species participated in the aging-induced metal-support interactions (indicated as red arrows) are highlighted with red borders. H<sub>2</sub> treatment (attempted regeneration) was not effective in reversing the sintering of 3% Pd/Al<sub>2</sub>O<sub>3</sub>, but did allow slight reactivation of the aged 3% Pd/CZO by “releasing” the Pd species from the Pd–O–Ce interaction assisted by the Pd<sup>x+</sup>/Pd<sup>0</sup> and Ce<sup>4+</sup>/Ce<sup>3+</sup> redox couples, by enhancing the redox efficiency. The electron current flowing between the metal and support redox couples is highlighted in purple. In any case, the metal-support effects were negligible compared to the metal sintering, with the latter being the primary cause of irreversible Pd-TWC deactivation during thermal oxidative aging.

### 3. Experimental Section

#### 3.1. Catalyst Materials

3% Pd/Al<sub>2</sub>O<sub>3</sub> and 3% Pd/Ce<sub>x</sub>O<sub>y</sub>-ZrO<sub>2</sub> (denoted as CZO with Ce:Zr atomic ratio of 1:2) were selected as model catalysts for the supported Pd component in automotive TWC. The catalysts and the reference support materials were supplied by BASF Iselin, NJ, USA. The catalysts were prepared by incipient wetness impregnation of the precursor salts (proprietary) onto the support (γ-Al<sub>2</sub>O<sub>3</sub> or CZO), followed by calcination in air at 550 °C for 2 h. The final catalyst sample had an average particle size of less than 30 μm, and was stored in ambient air.

#### 3.2. Catalyst Activity Tests after Aging and Attempted Regeneration

The fuel shutoff process was simulated by aging the fresh catalysts in air at 800 °C, 950 °C, or 1050 °C for a 5 min period. The aged catalysts were cooled to room temperature in ambient air. Attempted catalyst regeneration was performed by exposing the aged sample to a reducing atmosphere generated by SR with a mixture feed of 500 vppm propane, 10 vol % steam, 8 vol % CO<sub>2</sub>, and N<sub>2</sub> in balance. These tests were conducted at GHSV of 120,000 h<sup>-1</sup> at 550 °C for 1-h, simulating a slightly rich condition.

The catalyst regenerability was evaluated by measuring SR reforming activity at the same reaction feed as above with temperature scans from 200 °C to 550 °C, in 50 °C increments with a 30 min-hold at each temperature. The catalytic conversions were conducted far from the equilibrium.

#### 3.3. Catalyst Stability during Aging-Attempted Regeneration Cycle Tests

Catalytic cyclic tests (25 cycles in total) were performed to simulate the automotive engine operation cycles of oxidation (at fuel shutoff mode) followed by reduction (at fuel rich mode). The simulated fuel shutoff and rich conditions were maintained as described in Section 2.2, except the fuel shutoff temperature of 1050 °C was used. The catalytic SR activity after every five cycles were measured as described.

#### 3.4. Catalyst Characterization

The Brunauer-Emmett-Teller (BET) surface areas of the fresh and aged samples were determined using a *Quantachrome ChemBET Pulsar TPR/TPD* unit, equipped with a TCD detector. About 0.05 g of catalyst sample was outgassed in pure N<sub>2</sub> at 200 °C for 2 h, followed by N<sub>2</sub> adsorption performed with

30% N<sub>2</sub>/He. The TCD signal was calibrated using the external standard method, and the monolayer N<sub>2</sub> adsorption was evaluated by the single point BET approach.

The Transmission Electron Microscopic (TEM) images of the fresh, aged, and attempted regenerated samples were taken with a *JEOL 1400* TEM unit at Center of Functional Nanomaterial, Brookhaven National Lab. The TEM measurements were operated at an accelerating voltage of 120 kV. The catalyst powder sample was dispersed in pure ethanol (200 proof), followed by sonication for 3 h, and deposition on a Lacey carbon film supported Cu grid (200 mesh). For each sample, 50–60 TEM images with different magnifications at multiple spots were taken, and no less than 400 individual palladium particles were counted with *ImageJ* software. The mean surface area-weighted palladium particle size is calculated using Equation (1) [41]:

$$d_{TEM} = \frac{\sum_i n_i d_i^3}{\sum_i n_i d_i^2} \quad (1)$$

where  $n_i$  is the number of particles in Feret diameter  $d_i$  and  $\sum_i n_i > 400$ .

The XRD patterns of the fresh and aged catalysts were generated with a *PANalytical X'Pert<sup>3</sup> Powder XRD* unit. The powdered samples were single scanned between 15° and 90° with an incremental step of 0.01313° and a time per step of 300 s. The mean crystallite sizes  $d_s$  for the bulk  $\gamma$ -Al<sub>2</sub>O<sub>3</sub> and CZO support were determined with a precision of  $\pm 10\%$  from the line broadening of the most intense reflections using Scherrer's equation Equation (2) [5,28,42–45].

$$d_s = \frac{K\lambda}{\beta \cdot \cos \theta} \quad (2)$$

where  $\beta$  is the FWHM (full width at half maximum, in radians) of the selected diffraction peak,  $\theta$  (in radians) is the Bragg angle,  $K = 0.93$  is the numerical constant, and  $\lambda = 0.15406$  nm is the wavelength of the X-ray incident beam (Ni filtered Cu K $\alpha$ ).

The catalyst redox properties were studied by H<sub>2</sub>-Temperature Programmed Reduction (TPR). The measurements were carried out with the same *Quantachrome* unit as described above. About 0.1 g of catalyst sample was first outgassed in pure Helium at 150 °C for 2 h, and then cooled to room temperature. The TPR analysis was performed subsequently by heating the sample in a U-tube reactor to 800 °C at 5 °C/min in 4% H<sub>2</sub>/N<sub>2</sub>. Prior to TPR analysis, 4% H<sub>2</sub>/N<sub>2</sub> was purged in at ambient temperature for 30 min to achieve TPR baseline. The TCD signal (corresponding to H<sub>2</sub> uptake) was normalized per gram of catalyst.

#### 4. Conclusions

Both Rh and Pd components in automotive three way catalysts (TWC) experience deactivation during fuel shutoff through thermal oxidative aging (~1050 °C). A subsequent return to slightly rich of stoichiometric air-to-fuel ratio allows H<sub>2</sub> to be formed by steam reforming (SR) of engine exhaust HCs. Different deactivation and regeneration mechanisms occurred for Rh- and Pd-catalysts. Part I reported that the SR regeneration method was effective in reversing the deactivation of Rh-TWCs mainly by reducing and freeing the Rh from the metal-support interactions. Part II (the present paper) demonstrated that the attempted regeneration was not effective in recovering the activity of aged Pd-catalysts mainly due to extensive metal sintering. In summary,

- (1) Attempted *in situ* regeneration, through H<sub>2</sub> generation via catalytic steam reforming (SR), although effective for Rh catalysts, could not reverse the deactivation of Pd/Al<sub>2</sub>O<sub>3</sub> due to the severe metal sintering, but allowed a slight recovery of catalyst activity for Pd/CZO. For the latter catalyst, the enhanced redox between Pd<sup>x+</sup>/Pd<sup>0</sup> and Ce<sup>3+</sup>/Ce<sup>4+</sup> couples were likely promoting the catalytic SR regeneration.
- (2) Severe aging conditions also led to support sintering and some metal-support interactions for Pd–O–Ce. The metal support interaction had little effect on performance.
- (3) Metal re-dispersion by PdO reformation when cooled in air did not significantly occur due to the high degree of Pd sintering that occurred at 1050 °C.

In TWC, CO and HC oxidation activities will be greatly decreased by severe Pd sintering occurring during fuel shut off. It would be a breakthrough if PdO, the active state, could be stabilized against decomposition of Pd metal without the sacrifice of very much of its activity. A thermally stable PdO suggests that decreases in the amount of Rh in the current TWC might be possible since Pd has good NO<sub>x</sub> activity. Its high NO<sub>x</sub> activity was exploited in the mid-1990s when all Pd catalysts were commercialized in TWC when regulations were not as demanding as they are today.

### Acknowledgments

Financial support by BASF is greatly acknowledged. Meanwhile, the authors are grateful to the Shared Materials Characterization Lab at Columbia University for the XPS and XRD instruments, and Center of Functional Nanomaterials at Brookhaven National Lab for the TEM instrument. The authors would also like to thank Kim Kisslinger and Philip Rodenbough for the TEM training. Many thanks go to the lab assistances by Kyle Misquitta, Anh Nguyen, Yi Li, and Marcelle Lipman.

### Author Contributions

The present work was conducted under the supervision of Robert Farrauto, with Qinghe Zheng and Michel Deeba as authors at Columbia University and BASF in 2014–2015. Robert Farrauto did the main research consulting and paper editing, and is named the correspondent author of the submitted work. Qinghe Zheng (Ph.D. candidate) did the main experimental work (reactor tests and catalyst characterizations) and paper writing, and is named the primary author. Michel Deeba synthesized the catalyst materials and has been the project senior consultant.

### Conflicts of Interest

The authors declare no conflict of interest.

### References

1. Feng, H.; Lu, J.; Stair, P.C.; Elam, J.W. Alumina over-coating on Pd nanoparticle catalysts by Atomic Layer Deposition: Enhanced stability and reactivity. *Catal. Lett.* **2011**, *141*, 512–517.
2. Martí-Arias, A.; Fernández-García, M.; Iglesias-Juez, A.; Hungría, A.B.; Anderson, J.A.; Conesa, J.C.; Soria, J. Influence of thermal sintering on the activity for CO–O<sub>2</sub> and CO–O<sub>2</sub>–NO stoichiometric reactions over Pd/(Ce,Zr)O<sub>x</sub>/Al<sub>2</sub>O<sub>3</sub> catalysts. *Appl. Catal. B* **2002**, *38*, 151–158.

3. Martí-Arias, A.; Fernández-García, M.; Hungría, A.B.; Iglesias-Juez, A.; Duncan, K.; Smith, R.; Anderson, J.A.; Conesa, J.C.; Soria, J. Effect of thermal sintering on light-off performance of Pd/(Ce,Zr)O<sub>x</sub>/Al<sub>2</sub>O<sub>3</sub> three-way Catalysts: Model gas and engine tests. *J. Catal.* **2001**, *204*, 238–248.
4. Ivanova, A.S.; Slavinskaya, E.M.; Gulyaev, R.V.; Zaikovskii, V.I.; Stonkus, O.A.; Danilova, I.G.; Plyasova, L.M.; Polukhina, I.A.; Boronin, A.I. Metal-support interactions in Pt/Al<sub>2</sub>O<sub>3</sub> and Pd/Al<sub>2</sub>O<sub>3</sub> catalysts for CO oxidation. *Appl. Catal. B* **2010**, *97*, 57–71.
5. Gil, S.; Garcia-Vargas, J.M.; Liotta, L.F.; Pantaleo, G.; Ousmane, M.; Retailleau, L.; Giroir-Fendler, A. Catalytic oxidation of propene over Pd catalysts supported on CeO<sub>2</sub>, TiO<sub>2</sub>, Al<sub>2</sub>O<sub>3</sub> and M/Al<sub>2</sub>O<sub>3</sub> oxides (M = Ce, Ti, Fe, Mn). *Catalysts* **2015**, *5*, 671–689.
6. Yue, B.; Zhou, R.; Wang, Y.; Zheng, X. Influence of transition metals (Cr, Mn, Fe, Co and Ni) on the methane combustion over Pd/Ce-Zr/Al<sub>2</sub>O<sub>3</sub> catalyst. *Appl. Surf. Sci.* **2006**, *252*, 5820–5828.
7. Roiban, L.; Sorbier, L.; Pichon, C.; Pham-Huu, C.; Drillon, M.; Ersen, O. 3D-TEM investigation of the nanostructure of a σ-Al<sub>2</sub>O<sub>3</sub> catalyst support decorated with Pd nanoparticles. *Nanoscale* **2012**, *4*, 946–954.
8. Narui, K.; Yata, H.; Furuta, K.; Nishida, A.; Kohtoku, Y.; Matsuzaki, T. Effects of addition of Pt to PdO/Al<sub>2</sub>O<sub>3</sub> catalyst on catalytic activity for methane combustion and TEM observations of supported particles. *Appl. Catal. A* **1999**, *179*, 165–173.
9. Che, M.; Viedrine, J. (Eds.) *Characterization of Solid Materials and Heterogeneous Catalysts: From Structure to Surface Reactivity*; Wiley-VCH: Weinheim, Germany, 2012; Chapter 16, p. 664.
10. Hansen, T.W.; Delariva, A.T.; Challa, S.R.; Datye, A.K. Sintering of catalytic nanoparticles: Particle migration or Ostwald Ripening. *Acc. Chem. Res.* **2013**, *46*, 1720–1730.
11. Chen, X.; Cheng, Y.; Seo, C.Y.; Schwank, J.W.; McCabe, R.W. Aging, re-dispersion, and catalytic oxidation characteristics of model Pd/Al<sub>2</sub>O<sub>3</sub> automotive three-way catalysts. *Appl. Catal. B* **2015**, *163*, 499–509.
12. Farrauto, R.J.; Hobson, M.C.; Kennelly, T.; Waterman, E.M. Catalytic chemistry of supported palladium for combustion of methane. *Appl. Catal. A* **1992**, *81*, 227–237.
13. Datye, A.K.; Bravo, J.; Nelson, T.R.; Atanasova, P.; Lyubovsky, M.; Pfefferle, L. Catalyst microstructure and methane oxidation reactivity during the Pd↔PdO transformation on alumina supports. *Appl. Catal. A* **2000**, *198*, 179–196.
14. Farrauto, R.J.; Lampert, J.K.; Hobson, M.C.; Waterman, E.M. Thermal decomposition and reformation of PdO catalysis: Support effects. *Appl. Catal. B* **1995**, *6*, 263–270.
15. Jiang, J.C.; Pan, X.Q.; Graham, G.W.; McCabe, R.W.; Schwank, J. Microstructure of Pd/ceria-zirconia catalyst after high-temperature aging. *Catal. Lett.* **1998**, *53*, 37–42.
16. Chou, T.C.; Kennelly, T.; Farrauto, R.J. Praseodymium-palladium binary oxide, catalyst compositions containing the same, and methods of use. U.S. Patent WO1992018243 A1, 12 April 1991.
17. Heck, R.M.; Farrauto, R.J.; Gulati, S. *Catalytic Air Pollution Control: Commercial Technology*, 3rd ed.; John Wiley & Sons: Hoboken, NJ, USA, 2009; pp. 103–176.
18. Wu, X.; Xu, L.; Weng, D. The thermal stability and catalytic performance of Ce–Zr promoted Rh-Pd/γ-Al<sub>2</sub>O<sub>3</sub> automotive catalysts. *Appl. Surf. Sci.* **2004**, *221*, 375–383.

19. Han, Z.; Wang, J.; Yan, H.; Shen, M.; Wang, J.; Wang, W.; Yang, M. Performance of dynamic oxygen storage capacity, water-gas shift and steam reforming reactions over Pd-only three-way catalysts. *Catal. Today* **2010**, *158*, 481–489.
20. Yang, M.; Shen, M.; Wang, J.; Wen, J.; Zhao, M.; Wang, J.; Wang, W. Pd-supported interaction-defined selective redox activities in Pd–Ce<sub>0.7</sub>Zr<sub>0.3</sub>O<sub>2</sub>–Al<sub>2</sub>O<sub>3</sub> model three-way catalysts. *J. Phys. Chem. C* **2009**, *113*, 12778–12789.
21. Hinokuma, S.; Fujii, H.; Okamoto, M.; Ikeue, K.; Machida, M. Metallic Pd nanoparticles formed by Pd–O–Ce interaction: A reason for sintering-induced activation for CO oxidation. *Chem. Mater.* **2010**, *22*, 6183–6190.
22. Monte, R.D.; Fornasiero, P.; Kašpar, J.; Rumori, P.; Gubitosa, G.; Graziani, M. Pd/Ce<sub>0.6</sub>Zr<sub>0.4</sub>O<sub>2</sub>/Al<sub>2</sub>O<sub>3</sub> as advanced materials for three-way catalysts-Part 1. Catalyst characterisation, thermal stability and catalytic activity in the reduction of NO by CO. *Appl. Catal. B* **2000**, *24*, 157–167.
23. Bera, P.; Patil, K.C.; Jayaram, V.; Subbanna, G.N.; Hegde, M.S. Ionic dispersion of Pt and Pd on CeO<sub>2</sub> by combustion method: Effect of metal-ceria interaction on catalytic activities for NO reduction and CO and hydrocarbon oxidation. *J. Catal.* **2000**, *196*, 293–301.
24. Tauster, S.J. Strong Metal-support interactions. *Acc. Chem. Res.* **1987**, *20*, 389–394.
25. Wu, S.J.; de Jonghe, L.C. Sintering of nanophase  $\gamma$ -Al<sub>2</sub>O<sub>3</sub> powder. *J. Am. Ceram. Soc.* **1996**, *79*, 2207–2211.
26. Kwak, J.H.; Hu, J.; Lukaski, A.; Kim, D.H.; Szanyi, J.; Peden, C.H.F. Role of pentacoordinated Al<sup>3+</sup> ions in the high temperature phase transformation of  $\gamma$ -Al<sub>2</sub>O<sub>3</sub>. *J. Phys. Chem. C* **2008**, *112*, 9486–9492.
27. Kenevey, K.; Valdivieso, F.; Soustelle, M.; Pijolat, M. Thermal stability of Pd or Pt loaded Ce<sub>0.68</sub>Zr<sub>0.32</sub>O<sub>2</sub> and Ce<sub>0.50</sub>Zr<sub>0.50</sub>O<sub>2</sub> catalyst materials under oxidizing conditions. *Appl. Catal. B* **2001**, *29*, 93–101.
28. Liu, Y.; Ma, D.; Han, X.; Bao, X.; Frandsen, W.; Wang, D.; Su, D. Hydrothermal synthesis of microscale boehmite and gamma nanoleaves alumina. *Mater. Lett.* **2008**, *62*, 1297–1301.
29. Valecillos, J.; Rodríguez, D.; Méndez, J.; Solano, R.; González, C.; Acosta, T.; Sánchez, J.; Arteaga, G. Propane dehydrogenation over alumina-supported palladium and palladium-tin catalysts. *CIENCIA* **2006**, *14*, 125–134.
30. Zhao, B.; Yang, C.; Wang, Q.; Li, G.; Zhou, R.J. Influence of thermal treatment on catalytic performance of Pd/(Ce,Zr)O<sub>x</sub>–Al<sub>2</sub>O<sub>3</sub> three-way catalysts. *Alloys Compd.* **2010**, *494*, 340–346.
31. Lieske, H.; Völter, J. Pd redispersion by spreading of PdO in O<sub>2</sub> treated Pd/Al<sub>2</sub>O<sub>3</sub>. *J. Phys. Chem.* **1985**, *89*, 1841–1842.
32. Eberhardt, A.M.; Benvenuti, E.V.; Moro, C.C.; Tonetto, G.M.; Damiani, D.E. NO decomposition on PdMo/ $\gamma$ -Al<sub>2</sub>O<sub>3</sub> catalysts. *J. Mol. Catal. A* **2003**, *201*, 247–261.
33. Chang, T.C.; Chen, J.J.; Yeh, C.T. Temperature-Programmed Reduction and Temperature-Resolved Sorption Studies of Strong Metal-Support Interaction in supported palladium catalysts. *J. Catal.* **1985**, *96*, 51–57.
34. Luo, J.; Meng, M.; Xian, H.; Tu, Y.; Li, X.; Ding, T. The nanomorphology-controlled palladium-support interaction and the catalytic performance of Pd/CeO<sub>2</sub> catalysts. *Catal. Lett.* **2009**, *133*, 328–333.

35. Matam, S.K.; Otal, E.H.; Aguirre, M.H.; Winkler, A.; Ulrich, A.; Rentsch, D.; Weidenkaff, A.; Ferri, D. Thermal and chemical aging of model three-way catalyst Pd/Al<sub>2</sub>O<sub>3</sub> and its impact on the conversion of CNG vehicle exhaust. *Catal. Today* **2012**, *184*, 237–244.
36. Jen, H.-W.; Graham, G.W.; Chun, W.; McCabe, R.W.; Cuif, J.-P.; Deutsch, S.E.; Touret, O. Characterization of model automotive exhaust catalysts: Pd on ceria and ceria-zirconia supports. *Catal. Today* **1999**, *50*, 309–328.
37. Iglesias-Juez, A.; Martí-Arias, A.; Fernández-García, M. Metal-promoter interface in Pd/(Ce,Zr)O<sub>x</sub>/Al<sub>2</sub>O<sub>3</sub> catalyst: Effect of thermal aging. *J. Catal.* **2004**, *221*, 148–161.
38. Daley, R.A.; Christou, S.Y.; Efstathiou, A.M.; Anderson, J.A. Influence of oxychlorination treatments on the redox and oxygen storage and release properties of thermally aged Pd–Rh/Ce<sub>x</sub>Zr<sub>1-x</sub>O<sub>2</sub>/Al<sub>2</sub>O<sub>3</sub> model three-way catalysts. *App. Catal. B* **2005**, *60*, 117–127.
39. Binet, C.; Jadi, A.; Lavalley, J. Metal-Support Interaction in Pd/CeO<sub>2</sub> catalysts: Fourier-transform Infrared Studies of the effects of the reduction temperature and metal loading: Part 1—Catalysts prepared by the Microemulsion Technique. *J. Chem. Soc.* **1992**, *88*, 2079–2084.
40. Summers, J.C.; Ausen, S.A. Interaction of cerium oxide with noble metals. *J. Catal.* **1979**, *58*, 131–143.
41. Gómez-Quero, S.; Cárdenas-Lizana, F.; Keane, M.A. Effect of Metal Dispersion on the Liquid-Phase Hydrodechlorination of 2,4-Dichlorophenol over Pd/Al<sub>2</sub>O<sub>3</sub>. *Ind. Eng. Chem. Res.* **2008**, *47*, 6841–6853.
42. Yao, M.H.; Baird, R.J.; Kunz, F.W.; Hoost, T.E. An XRD and TEM investigation of the structure of alumina-supported ceria-zirconia. *J. Catal.* **2007**, *166*, 67–74.
43. Riguetto, B.A.; Damyanova, S.; Gouliev, G.; Marques, C.M.P.; Petrov, L.; Bueno, J.M.C. Surface behavior of alumina-supported Pt catalyst modified with cerium as revealed by X-ray Diffraction, X-ray Photoelectron Spectroscopy, and Fourier Transform Infrared Spectroscopy of CO Adsorption. *J. Phys. Chem. B* **2004**, *108*, 5349–5358.
44. Samain, L.; Jaworski, A.; Edén, M.; Ladd, D.M.; Seo, D.; Garcia-Garcia, F.J.; Häussermann, U. Structural analysis of highly porous  $\gamma$ -Al<sub>2</sub>O<sub>3</sub>. *J. Solid State Chem.* **2014**, *217*, 1–8.
45. He, H.; Gao, C. A general strategy for the preparation of carbon nanotubes and graphene oxide decorated with PdO nanoparticle in water. *Molecules* **2010**, *15*, 4679–4694.